THE JOURNAL OF PHYSICAL CHEMISTRY B

Article

pubs.acs.org/JPCB

Characterizing Anharmonic Vibrational Modes of Quinones with Two-Dimensional Infrared Spectroscopy

Jenée D. Cyran, Jacob M. Nite, and Amber T. Krummel*

Chemistry Department, Colorado State University, Fort Collins, Colorado 80523-1872, United States

Supporting Information

ABSTRACT: Two-dimensional infrared (2D IR) spectroscopy was used to study the vibrational modes of three quinones—benzoquinone, naphthoquinone, and anthraquinone. The vibrations of interest were in the spectral range of 1560−1710 cm^{-1}, corresponding to the in-plane carbonyl and ring stretching vibrations. Coupling between the vibrational modes is indicated by the cross peaks in the 2D IR spectra. The diagonal and off-diagonal anharmonicities range from 4.6 to 17.4 cm^{-1} for the quinone series. In addition, there is significant vibrational coupling between the in-plane carbonyl and ring stretching vibrations. The diagonal anharmonicity, off-diagonal anharmonicity, and vibrational coupling constants are reported for benzoquinone, naphthoquinone, and anthraquinone.

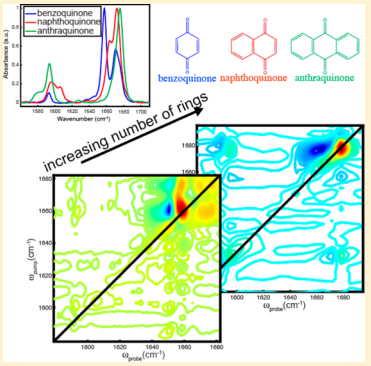

I. INTRODUCTION

Coherent multidimensional infrared spectroscopies, including 2D and 3D IR spectroscopy, have had a tremendous impact on investigations of solvent dynamics and structure conformational dynamics related to biological systems in the past decade.[1−5] In particular, 2D IR spectroscopy is now a robust tool for probing lipid membranes,[6,7] peptides,[8−10] and proteins.[11−13] Carbonyl groups are strong oscillators that have useful characteristics including being sensitive to local solvent environments, hydrogen bonding, and relative orientations of the oscillators.[14,15] Investigators take advantage of the localized nature of the transition dipole associated with the carbonyl stretching motion in biological molecules in order to monitor structural dynamics under varying conditions. For example, the carbonyl ester in phospholipids reports on the orientation of the phospholipid headgroup[16−18] and, of course, the amide I vibrations of peptides and proteins are used extensively.[19−23] 2D IR spectroscopy has also been extended to study nucleic acids, albeit to a lesser extent.[24−27] Four of the five nucleotides in DNA and RNA include carbonyl bonds that produce carbonyl stretch vibrations with strong oscillator strengths.[28] However, in the case of nucleic acids, spectral signatures from the carbonyl bonds are complicated by the fact that the transition dipole associated with the in-plane carbonyl stretch is not fully localized along the carbonyl bond but is somewhat delocalized onto the ring structure of the nucleotide base. Thus, prior to using the nucleotide carbonyl stretching vibration as a handle for probing structural dynamics, investigations instead have focused on fully characterizing the anharmonic vibrational modes in single nucleotides and developing models to describe the inter- and intramolecular vibrational coupling in nucleotides and model DNA oligomers.[24,29−31] In reality, there exist many biologically relevant molecules that contain hetero ring structures or highly conjugated ring structures, which may need to be treated similarly to the nucleotides. Quinones are one example of carbonyl containing conjugated ring structures that are ubiquitous in biology.

Quinone derivatives are important molecules in plant, microbial, and mammalian biology. The benzoquinone derivatives, plastoquinone, and ubiquinone are required for electron transfer in plant chloroplasts and mitochondrial membranes, respectively.[32,33] Naphthoquinone derivatives give rise to vitamin Ks that are required for post-translational modification of proteins required for blood coagulation and bone health.[34] In addition, anthraquinone derivatives make up drugs that are important in the treatment of malaria and cancer.[35,36] In each of these examples, the quinone performs its role in a complex, condensed phase environment. In order to fully characterize the role of quinones, one must be able to probe their structure and dynamics in their natural environments. 2D IR spectroscopy is particularly well suited to probe these molecules in their native environments because the spectroscopic experiments can be tailored to handle highly scattering media such as lipid membranes. However, extracting information regarding molecular structure and the surrounding solvent dynamics from a vibrational spectrum requires the vibrational eigenstates of a molecule to be well characterized in order to facilitate the interpretation of the spectral data. In this work, a series of quinones with increasing ring content are

Special Issue: Branka M. Ladanyi Festschrift

Received: July 10, 2014
Revised: February 16, 2015

DOI: 10.1021/jp506900n
J. Phys. Chem. B XXXX, XXX, XXX−XXX

investigated and the anharmonic vibrational modes are characterized.

Characteristics of molecular vibrational eigenstates generally fall between two limiting cases: At one limit, the vibrational eigenstates in a molecule can be considered harmonic, normal modes that are anharmonically coupled, and at the second limit, the vibrational eigenstates in a molecule can be considered anharmonic, local modes that are harmonically coupled.[37] In reality, many molecular systems, including the quinone series investigated here, have vibrational eigenstates that cannot be described perfectly by either of these limiting cases but instead lie in between these two limits. Thus, it is important to directly measure the characteristics of the molecular vibrational modes. It has been shown that one can naturally cross over from the first limit to the second limit, but the key parameter to consider is the ratio of vibrational coupling to the anharmonicity of the bond potentials. If vibrational coupling is large relative to the anharmonicity of the potential, the vibrational eigenstate is considered to be in the "near-normal" limit, whereas, if vibrational coupling is small relative to the anharmonicity of the potential, the vibrational eigenstate is considered to be in the "near-local" behavior.[38] Independent of where the vibrational eigenstates of quinones lie in between these limiting behaviors, the vibrational characteristics of quinones must be reported in order to use them to report on biological structure, dynamics, and function in the future. 2D IR spectroscopy probes the transitions between the ground, first, and second vibrational levels and is, thus, sensitive to vibrational coupling and anharmonicity. 2D IR spectroscopy also allows diagonal and off-diagonal anharmonicities to be observed directly, thereby providing a direct measure of vibrational anharmonicity. In this work, we characterize the anharmonic vibrational characteristics of the in-plane carbonyl stretching and in-plane ring deformations of three quinones: benzoquinone, naphthoquinone, and anthraquinone. The diagonal and off-diagonal anharmonicities of the observed absorption features are extracted from 2D IR spectra collected on this series of molecules. In addition, the magnitudes of vibrational couplings between the carbonyl and ring vibrations are determined.

II. EXPERIMENTAL AND COMPUTATIONAL METHODS

Linear IR and 2D IR Spectroscopy. The samples prepared for all linear IR absorption and 2D IR experiments have concentrations of 10.0 mM solute in chloroform. All samples were measured at room temperature and were placed between two CaF_2 plates with a 200-μm-thick Teflon spacer. 1,4-Benzoquinone was purchased from Sigma-Aldrich. 1,4-Naphthoquinone and 9,10-anthraquinone were purchased from Acros Organics. Chloroform (ACS grade) was used as the solvent for each sample and purchased from Fisher Scientific. Each sample was in monomeric form; this was confirmed by the lack of spectroscopic features indicative of aggregation in the UV−visible absorption and linear IR absorption spectroscopy experiments. For example, there were no shifts in the UV−vis absorption spectroscopy experiments collected as a function of quinone concentration from 5.0 to 20.0 mM.

Linear IR absorption spectra were collected using a Nicolet 6700 spectrometer (Thermo Fisher Scientific) with 4 cm^{-1} resolution and averaging 64 scans. The spectra were processed using the atmospheric suppression correction in the OMNIC software (Thermo Fisher Scientific). All linear IR absorption spectra have an air background subtracted; in addition, a percentage of chloroform background was subtracted to ensure solvent peaks were removed. Each linear IR absorption spectrum was baseline corrected by picking two end points and adjusting the end points to zero using a MATLAB program written in-house. The linear IR absorption data and slices extracted from the 2D IR data are fit with Gaussian line shapes using MATLAB minimization tools.

Each quinone sample was probed using 2D IR spectroscopy, where three mid-IR electric fields interact with the sample to generate an electric field that is the third-order signal. The 2D IR spectrometer used in these experiments consists of a Ti:sapphire oscillator used to seed a regenerative chirped pulse amplifier (Wyvern 1000, KM Laboratories) to produce sub-45 fs pulses at a 1 kHz repetition rate; the wavelength of these pulses is centered at 800 nm. The 800 nm pulses pump an optical parametric amplifier (OPA, Light Conversion TOPAS-C) with a difference frequency generation stage ($AgGaS_2$) used to produce tunable mid-IR light. The mid-IR pulses were centered at 6000 nm, had 9 μJ of energy, and were 70 fs in duration as determined by autocorrelation. A 90:10 beamsplitter was used to direct the majority of the IR light to a Ge-acoustic optic modulator (Ge-AOM, Isomet Corporation LS600-1109) based pulse shaper.[39,40] Direct pulse-shaping in the mid-IR is performed with active Bragg angle compensation being utilized. The details of active Bragg angle compensation can be found in ref 41 but are briefly described here. The pulse shaper is set up in a 4-*f* geometry. The mid-IR light is directed onto a grating with a groove density of 100 ln/mm. The diffracted beam is directed toward a cylindrical mirror (129.4 mm f.l.). A 3-in. gold mirror is used to direct the beam into the Ge-AOM at the Bragg angle. The beam is reflected off of identical optics in the second half of the zero dispersion compressor in order to complete the 4-*f* pulse shaper. An arbitrary waveform generator (AWG, DynamicSignals LLC PXDAC4800) is used to generate a Bragg angle compensated acoustic wave. The Bragg angle compensated waveform takes the instantaneous phase into account in order to perform a frequency sweep of the acoustic wave and thereby minimize angular dispersion in the pulse shaper.[41] The resulting shaped pulses are 134 fs in duration, as measured by autocorrelation. A pump−probe beam geometry was used where the beams are reflected off of a 90° parabolic mirror (101.6 mm f.l.). The third-order signal is self-heterodyned, since it follows the path of the probe beam after the sample and was detected using a linear 64-element mercury cadmium telluride (MCT) array detector. Signal to noise was improved by averaging 300 scans for each sample. The background scatter and transient absorption signals are subtracted from the signal by phase cycling the pump pulses.[42] The ω_{pump} axis of the 2D IR spectra is a Fourier transformation of τ_1, which is scanned from 0 to 2.5 ps in 7 fs steps with the pulse shaper. The ω_{probe} axis is obtained by dispersing the electric field of the third-order signal off of a grating in the monochromator and thus transforming the signal into the frequency domain. The ω_{probe} axis was calibrated using atmospheric water vapor. The logarithm of a purged spectrum divided by a nonpurged spectrum results in an absorption spectrum similar to a linear IR absorption spectrum. The result of the calibration determines the wavelength at each pixel of the spectrometer. The ω_{pump} axis is calibrated with a pump interference spectrum. The three mid-IR electric fields and the emitted electric field of the third-order signal are each polarized parallel to each other. In this experimental geometry, the absorptive 2D IR spectra are recorded.

DOI: 10.1021/jp506900n
J. Phys. Chem. B XXXX, XXX, XXX−XXX

Computational Methods. All three quinones investigated experimentally were also studied using theoretical calculations. Gas-phase geometry optimizations and frequency calculations were completed using density functional theory (DFT) with the Becke-3-Lee-Yang-Parr (B3LYP) exchange-correlation functional and second-order Møller–Plesset (MP2) perturbation theory. The basis sets used with each method were 6-31G(d) and 6-311G(d,p). For completeness, calculations were completed with and without the dielectric constant for chloroform. In addition, both harmonic and anharmonic frequency calculations were performed. All calculations were performed in Gaussian 09.[43] Only the data for the DFT B3LYP/6-311G(d,p) anharmonic calculations are included in Table 2. The scaling factor for B3LYP with 6-311G(d,p) is 0.9619.[44] This scaling factor was applied to the calculated frequencies.

III. RESULTS AND DISCUSSION

The molecular structure and linear IR absorption spectra of benzoquinone, naphthoquinone, and anthraquinone are shown in parts a–c of Figure 1, respectively. In the spectral region

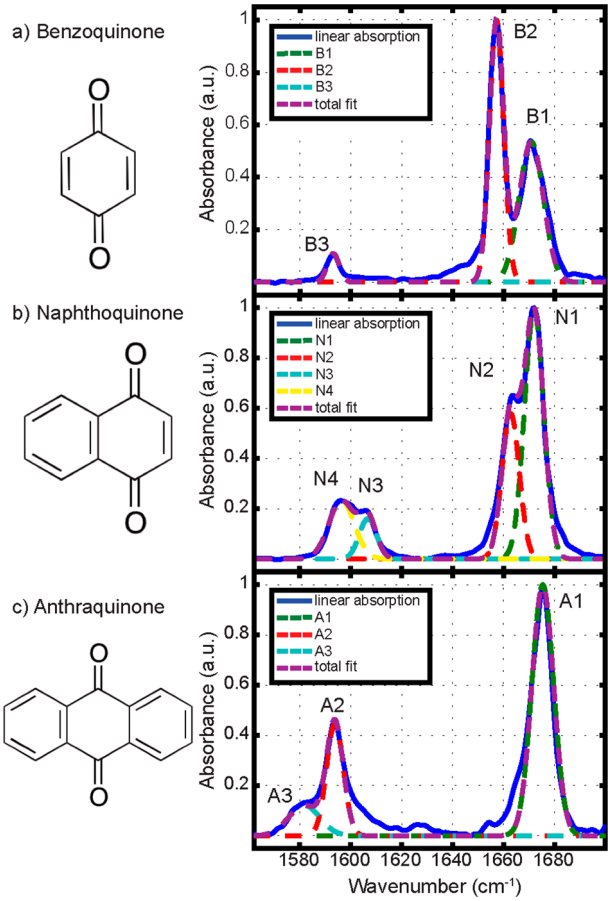

Figure 1. Molecular structures and linear spectra with Gaussian fits of benzoquinone, naphthoquinone, and anthraquinone in chloroform.

from 1560 to 1710 cm^{-1}, the peaks arise from carbonyl and ring vibrational modes. Traditionally, the lower frequency peaks have been assigned to in-plane ring deformation modes that are dominated by motion along the C=C bonds and the higher frequency peaks have been assigned to the in-plane C=O stretching vibrations.[45] However, other studies have resulted in different assignments for the peaks in the 1560–1710 cm^{-1} spectral region. For instance, studies of benzoquinone have reported the C=C stretching vibration as the higher frequency mode,[46] while others have attributed the higher frequency mode to a Fermi resonance.[47] The situation is similar for naphthoquinone and anthraquinone.[48] Thus, the description of the modes in the spectral region from 1560 to 1710 cm^{-1} continues to be debated and complete descriptions of these anharmonic vibrations are needed. As demonstrated in Figure 1, the linear IR absorption spectra varied significantly for this series of quinones. Hence, the linear data illustrates the potential for differences in the nuclear motions that contribute to the vibrational modes observed. As such, the traditional labeling of vibrational modes is likely unsuitable for describing the observed vibrational modes in this series of quinones. In order to avoid confusion and to assist in proper identification, the peaks will be referred to by the label, B1, B2, etc., throughout the paper. The labels for benzoquinone (B1–B3), naphthoquinone (N1–N4), and anthraquinone (A1-A3) are descriptions for the vibrational modes and are noted in Figure 1.

The peaks for benzoquinone (B1–B3), naphthoquinone (N1–N4), and anthraquinone (A1-A3), illustrated in Figure 1a–c, were fit using Gaussian lineshapes where the oscillator strengths, center frequency, and line widths were allowed to vary. The total fit indicated in purple is the sum of the contributing Gaussian fits. The results of these fits are summarized in Table 1.

With symmetrically positioned carbonyls on the molecule, if traditional peak assignments hold, there will be two normal modes in the 1650–1680 cm^{-1} spectral region due to

Table 1. Extracted Anharmonicities of Quinones from 2D IR Experiments

quinone	modes[a]	ω (cm^{-1})	$\Delta\omega^b$ (cm^{-1})	β^c (cm^{-1})
benzoquinone	B1	1670.9	7.6 ± 0.2	
	B2	1657.3	9.0 ± 0.2	
	B3	1593.1	4.6 ± 0.7	
	B1B2		6.2 ± 0.1	4.6
	B1B3		4.6 ± 0.2	23.6
	B2B3		5.7 ± 0.2	2.5
naphthoquinone	N1	1672.0	17.4 ± 1.0	
	N2	1662.8	13.7 ± 0.2	
	N3	1606.7	1.3[d]	
	N4	1596.4	12.9 ± 0.4	
	N1N2		17.1 ± 0.3	3.3
	N1N3		8.0[d]	2.9
	N1N4		12.9 ± 0.6	7.1
	N2N3		0.5[d]	3.2
	N2N4		8.2 ± 0.3	13.0
	N3N4		12.4[d]	5.9
anthraquinone	A1	1675.4	13.2 ± 0.2	
	A2	1593.8	6.0 ± 0.1	
	A3	1581.7	6.0[d]	
	A1A2		5.3 ± 0.5	11.8
	A1A3		4.0[d]	11.3
	A2A3		8.9[d]	7.3

[a]Normal mode labels are noted in Figure 1. [b]Anharmonicities extracted from Gaussian line shape fits of 2D IR slices in Figure 4 and the figures illustrated in the Supporting Information. [c]Vibrational coupling extracted from inverting the Hamiltonian. [d]Anharmonicity obtained from inverting the Hamiltonian for the numerical solution.

DOI: 10.1021/jp506900n
J. Phys. Chem. B XXXX, XXX, XXX–XXX

symmetric and antisymmetric stretches of the carbonyl vibrations. Each quinone in this series has vibrational modes within the spectral region from 1650 to 1680 cm^{-1}; however, there is significant variability in peak positions and intensities. Benzoquinone has two peaks, B1 and B2, with significant intensity. Naphthoquinone has two peaks, N1 and N2, with significant intensity. Anthraquinone has one peak, A1, within the spectral region from 1650 to 1680 cm^{-1} that has significant intensity. Anthraquinone and benzoquinone each have peaks in this region that appear as shoulders on the main peaks; these peaks that appear as shoulders are difficult to resolve from the main peaks and are not expected to contribute vibrational coupling in the molecules due to the weak oscillator strengths that they exhibit. The oscillator strength of each vibrational mode will depend on the extent of orthogonality between the vibrational modes; for example, if the vibrational modes are perpendicular, the oscillator strength will be held completely in either the symmetric or antisymmetric mode. The linear IR spectrum of anthraquinone suggests that anthraquinone is nearing the limit of having orthogonal vibrational modes in this region. This is in contrast to the linear spectra of benzoquinone and naphthoquinone that exhibit significant oscillator strength in both vibrational modes in the 1650−1680 cm^{-1} region.

Benzoquinone, naphthoquinone, and anthraquinone each have vibrations in the region from 1560 to 1620 cm^{-1} that have been traditionally assigned as symmetric and antisymmetric, in-plane ring deformations that are dominated by C═C bond motions. The lower frequency modes, B3, N3, N4, A2, and A3, exhibit no correlation between the number of rings and the transition dipoles in the lower frequency region. As seen in Figure 1, the spectral region from 1560 to 1710 cm^{-1} evolves from benzoquinone to anthraquinone with only the addition of rings: the peak positions and relative intensities change, thus indicating that each of these vibrational modes contains carbonyl stretching and ring deformation character. Moreover, the integrated intensity from 1560 to 1710 cm^{-1} remains approximately constant. Therefore, the relative magnitudes of ring deformation and carbonyl stretching character are varying between benzoquinone, naphthoquinone, and anthraquinone. The goal of this paper is to characterize the differences in the relationship between the ring and carbonyl modes as rings are added in this quinone series. To this end, the vibrational anharmonicity for each mode and the vibrational coupling between each mode will be reported.

In order to understand the mixing of the vibrational modes, 2D IR experiments were completed on benzoquinone, naphthoquinone, and anthraquinone; the spectra are plotted in Figure 2. The three transitions of interest in benzoquinone and the four transitions of interest in naphthoquinone occur between 1580 and 1680 cm^{-1} and thus can be probed simultaneously at a spectral resolution of 1.7 cm^{-1} with the spectrometer centered at 1629 cm^{-1}. The three transitions of interest in anthraquinone occur between 1560 and 1700 cm^{-1}; in order to probe these vibrations simultaneously, a grating with a lower groove density (75 lines/mm) was utilized in the 2D IR spectrometer, resulting in a spectral resolution of 5.4 cm^{-1}.

The 2D IR spectra presented here contain peaks along the diagonal and cross peaks that appear off of the diagonal; both types of features come as pairs of peaks. The peak pairs along the diagonal in Figure 2 are derived from the $v = 0$ to the $v = 1$ transition (positive in red) and the $v = 1$ to $v = 2$ transition (negative in blue). The pairs of peaks along the diagonal are separated along ω_{probe} by the anharmonicity, Δ_i, of the

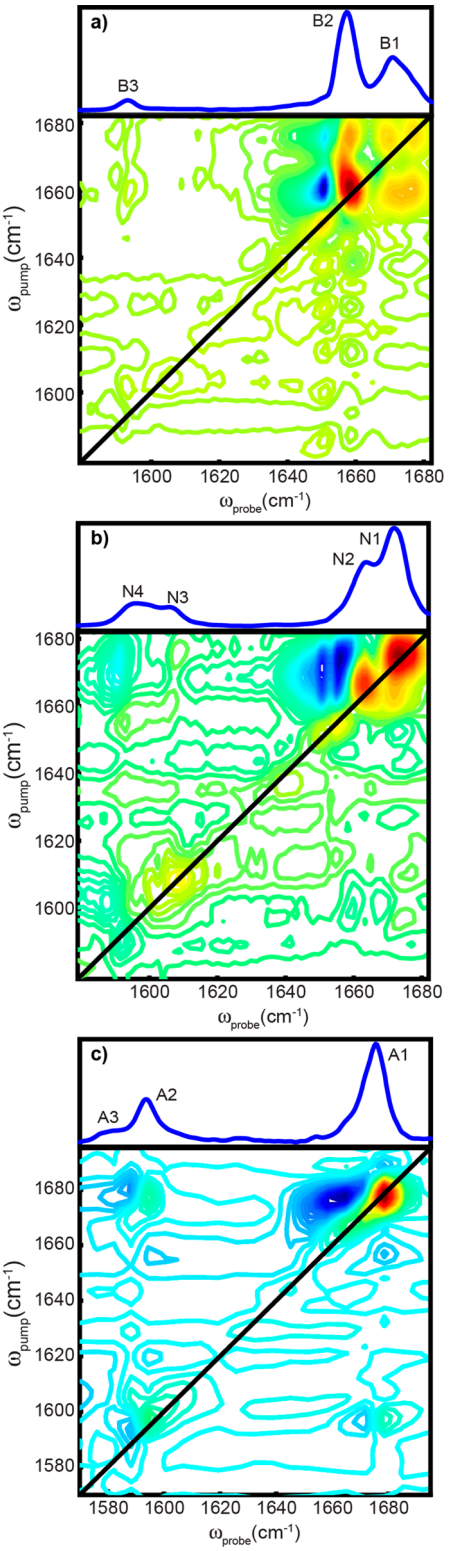

Figure 2. Linear and 2D IR spectra of the carbonyl and ring modes of (a) benzoquinone, (b) naphthoquinone, and (c) anthraquinone in chloroform. The 2D IR spectrum of benzoquinone is plotted in 1.8% intervals, and the 2D IR spectra of naphthoquinone and anthraquinone are plotted in 2.5% intervals.

vibrational mode. The cross peaks in the 2D IR spectra also have positive and negative peak pairs, where the pairs of peaks along ω_{probe} are separated by the off-diagonal anharmonicity, Δ_{ij}, of the vibrational modes that interact with each other. The

DOI: 10.1021/jp506900n
J. Phys. Chem. B XXXX, XXX, XXX−XXX

presence of cross peaks indicates vibrational coupling between two vibrational modes.

In a 2D IR spectrum, the intensity scales as $I \propto \mu_{0i}^4$ for the diagonal peaks and $I \propto \mu_{0i}^2 \mu_{ij}^2$ for the cross peaks. Thus, the diagonal and cross peaks will not necessarily have the same intensity. The intensity of the cross peaks pumped at a lower frequency is proportional to the square of the dipole strength of the lower frequency modes, which are less intense than the higher frequency modes for the data presented in Figure 2. Therefore, cross peaks pumped at lower frequencies are less intense than cross peaks pumped at higher frequencies.

The spectra in Figure 2 depict the full spectral range of interest from 1560 to 1700 cm^{-1}. However, the spectra in Figure 2 are congested in the higher frequency region, from 1650 to 1680 cm^{-1}. Therefore, 2D IR spectra were also collected of only the high frequency regions considered to be dominated by carbonyl stretching contributions to the vibrational modes. Figure 3 depicts the 2D IR spectra of the higher frequency modes collected at the highest spectral resolution of the spectrometer. The spectra of the carbonyl regions are collected with a spectral resolution of 1.7 cm^{-1}, and the spectrometer is centered at 1664 cm^{-1} for the series of quinones investigated here. This is specifically advantageous for anthraquinone, since the lowest spectral resolution of the spectrometer was used to acquire the spectrum in Figure 2c.

The spectra in Figures 2 and 3 illustrate coupling by the presence of cross peaks. In order to quantitatively describe the coupling of the vibrational modes, the Hamiltonian was inverted to obtain the vibrational coupling values. The diagonal, Δ_i, and off-diagonal, Δ_{ij}, anharmonicities were obtained from slices taken along the ω_{probe} axis from the 2D IR spectra. Representative ω_{probe}-axis slices are shown in Figure 4. The slices were taken from 2D IR spectra collected with a spectral resolution of 1.7 cm^{-1}. The slices were taken at different ω_{pump} positions corresponding to peak positions of the fundamental vibrational modes extracted from the linear IR absorption spectra. The slices along the ω_{probe} axis in Figure 4 are representative slices for each quinone and illustrate diagonal and cross peaks. A baseline correction was completed for each slice. The slices shown in Figure 4 were taken at ω_{pump} = 1671 cm^{-1}, ω_{pump} = 1596 cm^{-1}, and ω_{pump} = 1593 cm^{-1} for benzoquinone, naphthoquinone, and anthraquinone, respectively. The ω_{pump}-axis slices were fit with Gaussian lineshapes to obtain peak positions, full width at half-maximum (fwhm) line widths, and peak intensities. The fits were completed using the oscillator strength from the linear absorption spectra for the 0−1 transitions. Normalizing the intensity and taking the fourth root produces the oscillator strength for the slices. The oscillator strengths for the 0−1 transitions of the diagonal peaks in the slices are within 0.06 of the oscillator strengths obtained from the linear absorption spectra. The 1−2 transitions were fit on the basis of the integrated intensity of the 0−1 transition. Therefore, the peak area for the 0−1 transition is the same as the peak area for the 1−2 transition for each peak pair. The slices were taken from both Figures 2 and 3 to extract the peak positions. Figure 3 contains spectra of only the high frequency modes. Therefore, the slices from Figure 3 are used to extract the higher frequency peak positions with less ambiguity. All slices and fully tabulated results can be found in the Supporting Information. The peak positions are used to calculate anharmonicities. The diagonal and off-diagonal anharmonicities are calculated by taking the difference in energies of the positive and negative peak pairs along the ω_{probe} axis. The

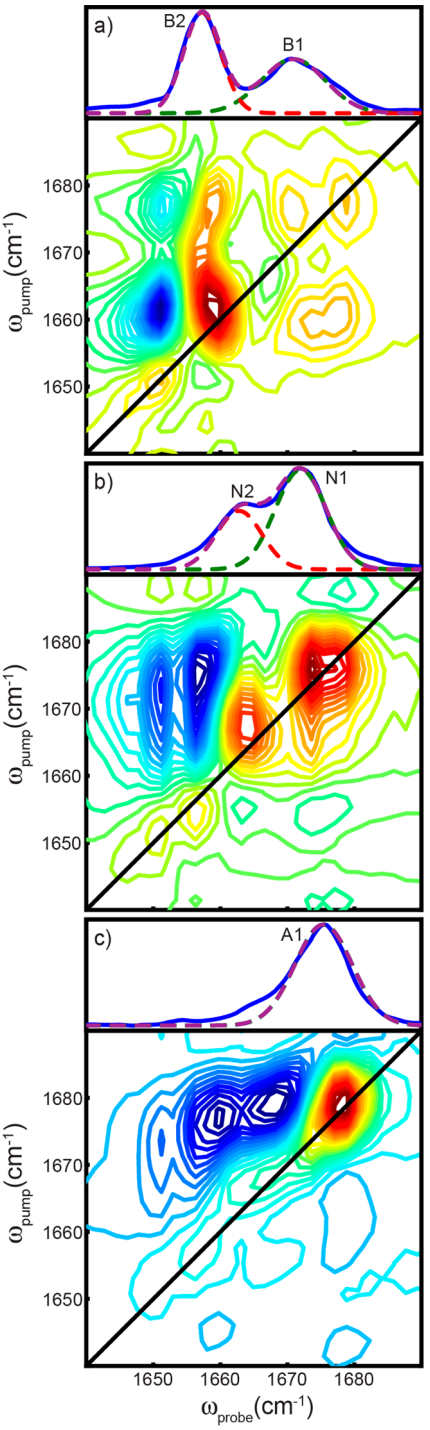

Figure 3. Linear and 2D IR spectra of the high frequency modes of (a) benzoquinone, (b) naphthoquinone, and (c) anthraquinone in chloroform. The 2D IR spectrum of benzoquinone is plotted in 3.3% intervals, and the 2D IR spectra of naphthoquinone and anthraquinone are plotted in 4.0% intervals.

anharmonicities are used as starting parameters for the numerical solution of the Hamiltonians. Unfortunately, one diagonal anharmonicity (Δ_{N3}) and five off-diagonal anharmonicities (Δ_{N1N3}, Δ_{N2N3}, Δ_{N3N4}, Δ_{A2A3}, Δ_{A1A3}) cannot be determined from these experiments due to spectral congestion and weak oscillator strengths. However, the diagonal and off-diagonal anharmonicities can also be determined by inverting

DOI: 10.1021/jp506900n
J. Phys. Chem. B XXXX, XXX, XXX−XXX

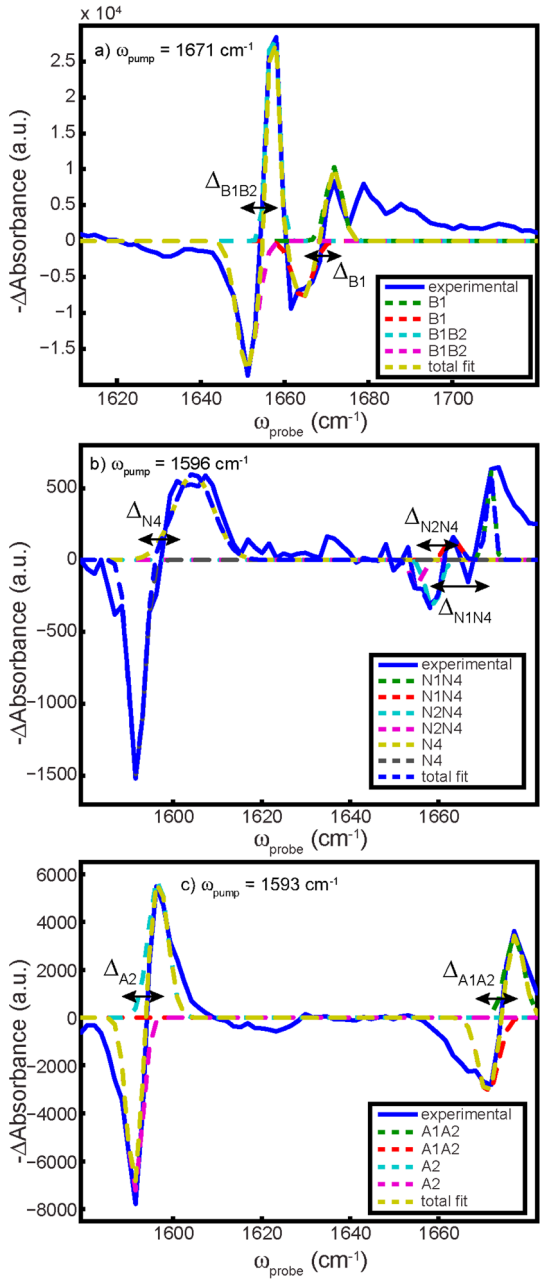

Figure 4. Representative slices along the ω_{probe} axis from the 2D IR spectra presented with fits to each peak pair for benzoquinone, naphthoquinone, and anthraquinone in chloroform. These slices illustrate both diagonal and cross peaks from which diagonal and off-diagonal anharmonicities were extracted.

the 2-Quantum Hamiltonian. The diagonal or off-diagonal anharmonicities are given in Table 1.

A platform for comparing the quinones in this series is provided now that the anharmonic characteristics of the vibrational modes in the 1560−1700 cm^{-1} region have been quantified. In this series, benzoquinone and anthraquinone are symmetric molecules, whereas naphthoquinone is asymmetric. In the symmetric benzoquinone and anthraquinone, the high frequency modes have larger diagonal anharmonicities than the low frequency modes. In contrast, the diagonal anharmonicities of the high frequency and low frequency modes are similar in the asymmetric naphthoquinone. These observations have implications on the localized nature of the vibration as well as whether or not these vibrational modes can be depicted by one of the two limiting cases noted above, namely, the "near-normal" mode or "near-local" mode pictures. In order to complete the characterization of these vibrational modes in this series of quinones, the magnitude of vibrational coupling between the low and high frequency vibrational modes must be considered.

Inverting the Hamiltonian is one way to calculate the vibrational couplings. The Hamiltonian was inverted by assuming degenerate carbonyl energies and degenerate ring energies for each quinone. The coupling constants were varied until the normal mode energies matched the fundamental frequencies obtained from the linear absorption spectra. The problem with this approach is that the intensities of the transition dipoles are not taken into account. To properly account for the intensities of the transition dipoles, polarization must be completed to find the angle of the transition dipoles.

The vibrational coupling calculated by inverting the Hamiltonian is reported in Table 1 for each quinone. For benzoquinone, the vibrational coupling between B1 and B3 is 23.6 cm^{-1}, and between B2 and B3, it is 2.5 cm^{-1}. For naphthoquinone, the vibrational coupling between N1 and N3 is 2.9 cm^{-1}, that between N1 and N4 is 7.1 cm^{-1}, that between N2 and N3 is 3.2 cm^{-1}, and that between N2 and N4 is 13.0 cm^{-1}. For anthraquinone, the vibrational coupling between A1 and A2 is 11.8 cm^{-1}, that between A1 and A3 is 11.3 cm^{-1}, and that between A2 and A3 is 7.3 cm^{-1}. The magnitudes of the vibrational coupling constants determined from the experiments presented in this work are comparable to the magnitudes of the vibrational coupling between in-plane ring deformation and carbonyl stretching modes in the bases of nucleic acids.[30] For each quinone in this series, the magnitudes of the vibrational coupling between the high and low frequency modes considered are large relative to the diagonal anharmonicities of each mode. This result is perhaps not surprising, considering the extent to which the carbonyl bond stretching motion could be mechanically coupled to the in-plane ring stretching motions in these quinones. The magnitudes of the vibrational coupling constants are large relative to the anharmonicities extracted; thus, the vibrational modes probed in this work are tending toward the "near-normal" mode limit.

The magnitudes of the vibrational coupling between two of the high frequency vibrational modes present in benzoquinone were also determined from these experiments. The vibrational coupling constant that describes the interaction between modes B1 and B2 in benzoquinone is equal to 4.6 cm^{-1}. The magnitude of the vibrational coupling constant is of the same order of the diagonal anharmonicities of the modes contributing to the interaction. In this situation, it is difficult to determine the extent to which the vibrational motion is delocalized from the carbonyl stretch across the in-plane ring motions.

The coupling between naphthoquinone modes N1 and N2 extracted from inverting the Hamiltonian is 3.3 cm^{-1}. The magnitude of the vibrational coupling constant is not of the same order of the diagonal anharmonicities of the modes contributing to the interaction. The zero, first, and second energies from the numerical solution are illustrated in Figure 5.

Having quantified the diagonal and off-diagonal anharmonicities for benzoquinone, naphthoquinone, and anthraquinone, energy level diagrams for each quinone can be generated. In Figure 5, energy level diagrams are shown for benzoquinone,

DOI: 10.1021/jp506900n
J. Phys. Chem. B XXXX, XXX, XXX−XXX

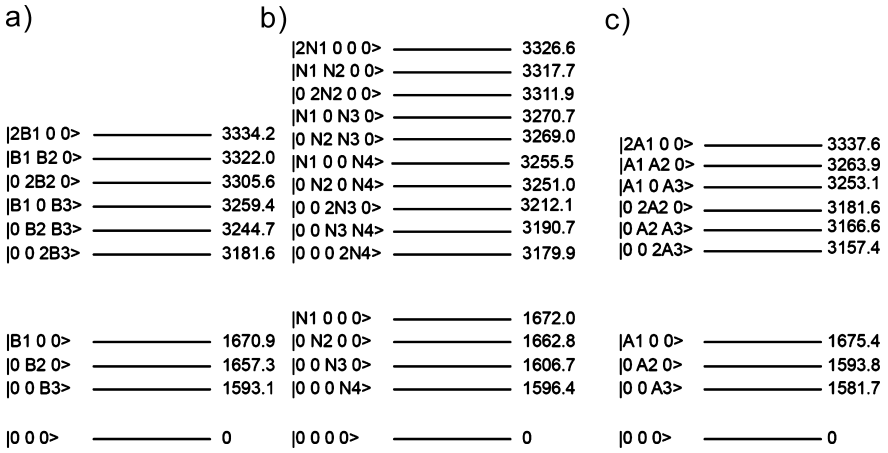

Figure 5. Energy level diagrams illustrating the zero, first, and second vibrational energy levels of (a) benzoquinone, (b) naphthoquinone, and (c) anthraquinone. The $v = 2$ states are calculated from using the anharmonicities shown in Table 1.

Table 2. Comparison of Experimental and Theoretical Results

	experimental[a]		DFT/6-311G(d,p)		
peak	ω (cm^{-1})	μ^b	ω (cm^{-1})	μ^b	vibrations[c]
			Benzoquinone		
B1	1670.9	0.72	1643.3	1.00	C═O(asym), C═C, C—C
B2	1657.3	1.00	1646.1	0.01	C═O(sym), C═C, C—C
B3	1593.1	0.33	1578.0	0.01	C═C, C—C
			Naphthoquinone		
N1	1672.0	1.00	1641.2	1.00	C═O(asym), C═C, C—C
N2	1662.8	0.78	1638.6	0.16	C═O(sym), C═C, C—C
N3	1606.7	0.40	1568.9	0.29	C═C, C—C
N4	1596.4	0.48	1539.8	0.37	C═O(sym), C═C, C—C
			Anthraquinone		
A1	1675.4	1.00	1647.9	1.00	C═O(asym), C═C, C—C
A2	1593.8	0.67	1538.9	0.00	C═C, C—C
A3	1581.7	0.35	1534.5	0.63	C═O(asym), C═C, C—C

[a]The experimental data is from the linear fits in Figure 1. [b]The dipole strengths are calculated from the square root of the normalized intensities. [c]The vibrations are obtained from the calculations and are the major contributors to each mode.

naphthoquinone, and anthraquinone. The energy diagrams illustrated in Figure 5 are the relevant energy levels for each quinone probed with 2D IR spectroscopy. The $v = 2$ energy states were calculated using the 0−1 transition energy and the anharmonicity extracted from the 2D IR spectra. The anharmonicities involving N3 and A3 could not be extracted from the 2D IR spectra; the anharmonicities from inverting the 2-Quantum Hamiltonian were used for transitions involving N3 and A3.

IV. COMPARING EXPERIMENT AND THEORY

Along with the linear IR absorption and 2D IR spectroscopy experiments, the quinones in this series were also studied using quantum mechanical calculations. The center vibrational frequencies and oscillator strengths obtained by fitting the linear IR absorption data can be compared to the calculated vibrational frequencies and oscillator strengths for each vibrational mode considered in this work. Benzoquinone and anthraquinone have three vibrational modes to consider, while naphthoquinone has four vibrational modes to consider in the spectral region from 1560 to 1700 cm^{-1} corresponding to the modes labeled in Figure 1. The parameters from the fits in Figure 1 are found in Table 2. The peak intensities are converted into dipole strength according to the scaling $I \propto \mu^2$.[49] The relative oscillator strengths and the center vibrational frequencies from the linear experimental data are compared to the theoretical data for each normal mode of interest. In general, the high frequency modes are known to be dominated by the carbonyl stretching motion and the low frequency modes are dominated by in-plane ring deformations involving C═C and C—C stretching motions.

In this series of quinones, benzoquinone and anthraquinone are highly symmetric molecules, which is in contrast to naphthoquinone. There are significant differences between the experimental and theoretical data with most of the differences occurring in the data related to benzoquinone and anthraquinone. In order to avoid using symmetry arguments to improve the speed of these calculations and thus potentially bias the results of the quantum mechanical calculations, the no symmetry condition in Gaussian 09 was applied. The vibrational frequencies and oscillator strengths from anharmonic frequency calculations for each quinone are provided in Table 2. Comparing observables including relative oscillator strengths and energies of each mode, one can quickly notice the deviation between the experimental and theoretical data.

In the symmetric quinones, benzoquinone and anthraquinone, the frequencies of the vibrations calculated are reasonable comparisons to the center frequencies of the observed modes.

DOI: 10.1021/jp506900n
J. Phys. Chem. B XXXX, XXX, XXX−XXX

The calculated vibrations are in better agreement for the higher frequency transitions than the lower frequency transitions within the spectral region from 1560 to 1700 cm^{-1}. The anthraquinone calculations correctly estimate the high frequency modes to carry the greatest oscillator strength, but one of the vibrational frequencies is estimated to carry no oscillator strength. The calculated oscillator strengths for benzoquinone significantly deviate from experiment.

In contrast to benzoquinone and anthraquinone, the theoretical vibrational frequency calculations of naphthoquinone agree quite well with the experimentally observed vibrational modes. The DFT calculation closely resembles the center frequencies and relative oscillator strengths observed for naphthoquinone. The 6-311G(d,p) basis set improves the center frequencies and maintains reasonable oscillator strengths. Inspection of the magnitudes of the nuclear motion in the four vibrational modes of interest provides insight as to why there is good agreement between theory and experiment in the case of naphthoquinone. The vibrational modes calculated for naphthoquinone each contain carbonyl stretching character and in-plane ring deformation character. Thus, the extent of delocalization or mixing of modes is better estimated in the theoretical calculations of naphthoquinone. It is important to note that performing these calculations with the addition of the dielectric constant for the chloroform solvent did not change the essential results for each quinone calculation.

V. CONCLUSIONS

2D IR spectroscopy provides a means to directly measure the anharmonic characteristics of quinone vibrational modes that lie between 1560 and 1710 cm^{-1}. Benzoquinone, naphthoquinone, and anthraquinone each have vibrational modes that lie in this region which are generally attributed to carbonyl stretching vibrations at high frequencies and in-plane ring deformations at lower frequencies. The diagonal and off-diagonal anharmonicities were quantified for the quinones investigated in this work. Subsequently, the magnitudes of the vibrational coupling constants between the high and low frequency modes were estimated. 2D IR measurements illustrate the delocalization of the ring and carbonyl contributions to quinone vibrational modes between 1560 and 1710 cm^{-1}. The characterization of the quinones in this paper relied solely on the experimental analysis from the linear and 2D IR spectra due to the differences between theoretical frequency calculations and the experimental results. However, it is important to note in the case of these quinones that, as the vibrations become more localized or the symmetry of the molecule is decreased, the agreement between the theoretical calculations and the experiments presented here is improved. Certainly work toward determining the relative orientation of the vibrational transition dipoles in these quinones needs to be completed. To this end, we are currently implementing polarization control in our 2D IR spectrometer. The characterization of the quinones in this paper provides an important picture of the vibrational states in the region between 1560 and 1710 cm^{-1}. Moreover, understanding the manner in which anharmonicity and vibrational coupling contributes to the mixing of contributions from the in-plane ring deformations and carbonyl stretching vibrations in quinones forms the foundation to investigating quinone derivatives, such as plastoquinone and vitamin K.

■ ASSOCIATED CONTENT

Supporting Information

Details regarding the fit parameters for the slices through the 2D IR spectra and figures of each slice taken along the ω_{probe} axis. This material is available free of charge via the Internet at http://pubs.acs.org.

■ AUTHOR INFORMATION

Corresponding Author

*E-mail: amber.krummel@colostate.edu.

Notes

The authors declare no competing financial interest.

■ ACKNOWLEDGMENTS

The authors thank Tony Rappé for access to their cluster and helpful discussions regarding the Gaussian calculations. We also wish to thank Melissa Reynolds for open access to the linear IR absorption and UV−visible absorption spectrometers. A.T.K. appreciates the generous funding for this work from the ACS Petroleum Research Fund (grant #51228-DNI6)

■ ABBREVIATIONS

IR, infrared; 2D IR, two-dimensional infrared; MP2, Møller−Plesset second-order perturbation theory; DFT, density functional theory; B3LYP, Becke-3-Lee-Yang-Parr

■ REFERENCES

(1) Ghosh, A.; Remorino, A.; Tucker, M. J.; Hochstrasser, R. M. 2D IR Photon Echo Spectroscopy Reveals Hydrogen Bond Dynamics of Aromatic Nitriles. *Chem. Phys. Lett.* **2009**, *469*, 325−330.

(2) Fayer, M. D. Dynamics of Liquids, Molecules, and Proteins Measured with Ultrafast 2D IR Vibrational Echo Chemical Exchange Spectroscopy. *Annu. Rev. Phys. Chem.* **2009**, *60*, 21−38.

(3) Demirdöven, N.; Cheatum, C. M.; Chung, H. S.; Khalil, M.; Knoester, J.; Tokmakoff, A. Two-Dimensional Infrared Spectroscopy of Antiparallel B-Sheet Secondary Structure. *J. Am. Chem. Soc.* **2004**, *126*, 7981−7990.

(4) Moran, S. D.; Woys, A. M.; Buchanan, L. E.; Bixby, E.; Decatur, S. M.; Zanni, M. T. Two-Dimensional IR Spectroscopy and Segmental 13C Labeling Reveals the Domain Structure of Human γD-Crystallin Amyloid Fibrils. *Proc. Natl. Acad. Sci. U. S. A.* **2012**, *109*, 3329−3334.

(5) Garrett-Roe, S.; Perakis, F.; Rao, F.; Hamm, P. Three-Dimensional Infrared Spectroscopy of Isotope-Substituted Liquid Water Reveals Heterogeneous Dynamics. *J. Phys. Chem. B* **2011**, *115*, 6976−6984.

(6) Osborne, D. G.; Dunbar, J. A.; Lapping, J. G.; White, A. M.; Kubarych, K. J. Site-Specific Measurements of Lipid Membrane Interfacial Water Dynamics with Multidimensional Infrared Spectroscopy. *J. Phys. Chem. B* **2013**, *117*, 15407−15414.

(7) Ghosh, A.; Wang, J.; Moroz, Y. S.; Korendovych, I. V.; Zanni, M.; DeGrado, W. F.; Gai, F.; Hochstrasser, R. M. 2D IR Spectroscopy Reveals the Role of Water in the Binding of Channel-Blocking Drugs to the Influenza M2 Channel. *J. Chem. Phys.* **2014**, *140*, 235105.

(8) Lessing, J.; Roy, S.; Reppert, M.; Baer, M.; Marx, D.; Jansen, T. L. C.; Knoester, J.; Tokmakoff, A. Identifying Residual Structure in Intrinsically Disordered Systems: A 2D IR Spectroscopic Study of the GVGXPGVG Peptide. *J. Am. Chem. Soc.* **2012**, *134*, 5032−5035.

(9) Sengupta, N.; Maekawa, H.; Zhuang, W.; Toniolo, C.; Mukamel, S.; Tobias, D. J.; Ge, N.-H. Sensitivity of 2D IR Spectra to Peptide Helicity: A Concerted Experimental and Simulation Study of an Octapeptide. *J. Phys. Chem. B* **2009**, *113*, 12037−12049.

(10) Hamm, P.; Lim, M.; DeGrado, W. F.; Hochstrasser, R. M. The Two-Dimensional IR Nonlinear Spectroscopy of a Cyclic Penta-Peptide in Relation to Its Three-Dimensional Structure. *Proc. Natl. Acad. Sci. U. S. A.* **1999**, *96*, 2036−2041.

DOI: 10.1021/jp506900n
J. Phys. Chem. B XXXX, XXX, XXX−XXX

(11) Bredenbeck, J.; Helbing, J.; Nienhaus, K.; Nienhaus, G. U.; Hamm, P. Protein Ligand Migration Mapped by Nonequilibrium 2D-IR Exchange Spectroscopy. *Proc. Natl. Acad. Sci. U. S. A.* **2007**, *104*, 14243−14248.
(12) Mukherjee, P.; Kass, I.; Arkin, I. T.; Zanni, M. T. Picosecond Dynamics of a Membrane Protein Revealed by 2D IR. *Proc. Natl. Acad. Sci. U. S. A.* **2006**, *103*, 3528−3533.
(13) Ishikawa, H.; Kim, S.; Kwak, K.; Wakasugi, K.; Fayer, M. D. Disulfide Bond Influence on Protein Structural Dynamics Probed with 2D-IR Vibrational Echo Spectroscopy. *Proc. Natl. Acad. Sci. U. S. A.* **2007**, *104*, 19309−19314.
(14) Kim, Y. S.; Hochstrasser, R. M. Applications of 2D IR Spectroscopy to Peptides, Proteins, and Hydrogen-Bond Dynamics†. *J. Phys. Chem. B* **2009**, *113*, 8231−8251.
(15) Baiz, C. R.; McRobbie, P. L.; Anna, J. M.; Geva, E.; Kubarych, K. J. Two-Dimensional Infrared Spectroscopy of Metal Carbonyls. *Acc. Chem. Res.* **2009**, *42*, 1395−1404.
(16) Volkov, V. V.; Chelli, R.; Zhuang, W.; Nuti, F.; Takaoka, Y.; Papini, A. M.; Mukamel, S.; Righini, R. Electrostatic Interactions in Phospholipid Membranes Revealed by Coherent 2D IR Spectroscopy. *Proc. Natl. Acad. Sci. U. S. A.* **2007**, *104*, 15323−15327.
(17) Zhao, W.; Moilanen, D. E.; Fenn, E. E.; Fayer, M. D. Water at the Surfaces of Aligned Phospholipid Multibilayer Model Membranes Probed with Ultrafast Vibrational Spectroscopy. *J. Am. Chem. Soc.* **2008**, *130*, 13927−13937.
(18) Costard, R.; Greve, C.; Heisler, I. A.; Elsaesser, T. Ultrafast Energy Redistribution in Local Hydration Shells of Phospholipids: A Two-Dimensional Infrared Study. *J. Phys. Chem. Lett.* **2012**, *3*, 3646−3651.
(19) Hamm, P.; Lim, M.; Hochstrasser, R. M. Structure of the Amide I Band of Peptides Measured by Femtosecond Nonlinear-Infrared Spectroscopy. *J. Phys. Chem. B* **1998**, *102*, 6123−6138.
(20) Ham, S.; Cho, M. Amide I Modes in the N-Methylacetamide Dimer and Glycine Dipeptide Analog: Diagonal Force Constants. *J. Chem. Phys.* **2003**, *118*, 6915−6922.
(21) DeCamp, M. F.; DeFlores, L.; McCracken, J. M.; Tokmakoff, A.; Kwac, K.; Cho, M. Amide I Vibrational Dynamics of N-Methylacetamide in Polar Solvents: The Role of Electrostatic Interactions. *J. Phys. Chem. B* **2005**, *109*, 11016−11026.
(22) Lin, Y.-S.; Shorb, J. M.; Mukherjee, P.; Zanni, M. T.; Skinner, J. L. Empirical Amide I Vibrational Frequency Map: Application to 2D-IR Line Shapes for Isotope-Edited Membrane Peptide Bundles†. *J. Phys. Chem. B* **2009**, *113*, 592−602.
(23) Bagchi, S.; Falvo, C.; Mukamel, S.; Hochstrasser, R. M. 2D-IR Experiments and Simulations of the Coupling between Amide-I and Ionizable Side Chains in Proteins: Application to the Villin Headpiece. *J. Phys. Chem. B* **2009**, *113*, 11260−11273.
(24) Krummel, A. T.; Mukherjee, P.; Zanni, M. T. Inter and Intrastrand Vibrational Coupling in DNA Studied with Heterodyned 2D-IR Spectroscopy. *J. Phys. Chem. B* **2003**, *107*, 9165−9169.
(25) Elsaesser, T. Two-Dimensional Infrared Spectroscopy of Intermolecular Hydrogen Bonds in the Condensed Phase. *Acc. Chem. Res.* **2009**, *42*, 1220−1228.
(26) Dwyer, J. R.; Szyc, Ł.; Nibbering, E. T. J.; Elsaesser, T. Ultrafast Vibrational Dynamics of Adenine-Thymine Base Pairs in DNA Oligomers. *J. Phys. Chem. B* **2008**, *112*, 11194−11197.
(27) Yang, M.; Szyc, Ł.; Röttger, K.; Fidder, H.; Nibbering, E. T. J.; Elsaesser, T.; Temps, F. Dynamics and Couplings of N−H Stretching Excitations of Guanosine−Cytidine Base Pairs in Solution. *J. Phys. Chem. B* **2011**, *115*, 5484−5492.
(28) Mantsch, H. H.; Chapman, D. *Infrared Spectroscopy of Biomolecules*; Wiley-Liss: New York, 1996.
(29) Krummel, A. T.; Zanni, M. T. Evidence for Coupling between Nitrile Groups Using DNA Templates: A Promising New Method for Monitoring Structures with Infrared Spectroscopy. *J. Phys. Chem. B* **2008**, *112*, 1336−1338.
(30) Peng, C. S.; Jones, K. C.; Tokmakoff, A. Anharmonic Vibrational Modes of Nucleic Acid Bases Revealed by 2D IR Spectroscopy. *J. Am. Chem. Soc.* **2011**, *133*, 15650−15660.
(31) Lee, C.; Park, K.-H.; Cho, M. Vibrational Dynamics of DNA. I. Vibrational Basis Modes and Couplings. *J. Chem. Phys.* **2006**, *125*, 114508.
(32) Allen, J. F.; Bennett, J.; Steinback, K. E.; Arntzen, C. J. Chloroplast Protein Phosphorylation Couples Plastoquinone Redox State to Distribution of Excitation Energy between Photosystems. *Nature* **1981**, *291*, 25−29.
(33) Kussmaul, L.; Hirst, J. The Mechanism of Superoxide Production by NADH:ubiquinone Oxidoreductase (complex I) from Bovine Heart Mitochondria. *Proc. Natl. Acad. Sci. U. S. A.* **2006**, *103*, 7607−7612.
(34) Morris, D. P.; Stevens, R. D.; Wright, D. J.; Stafford, D. W. Processive Post-Translational Modification Vitamin K-Dependent Carboxylation of a Peptide Substrate. *J. Biol. Chem.* **1995**, *270*, 30491−30498.
(35) Winter, R. W.; Cornell, K. A.; Johnson, L. L.; Isabelle, L. M.; Hinrichs, D. J.; Riscoe, M. K. Hydroxy-Anthraquinones as Antimalarial Agents. *Bioorg. Med. Chem. Lett.* **1995**, *5*, 1927−1932.
(36) El-Gogary, T. M. Molecular Complexes of Some Anthraquinone Anti-Cancer Drugs: Experimental and Computational Study. *Spectrochim. Acta, Part A* **2003**, *59*, 1009−1015.
(37) Child, M. S.; Lawton, R. T. Local and Normal Vibrational States: A Harmonically Coupled Anharmonic-Oscillator Model. *Faraday Discuss. Chem. Soc.* **1981**, *71*, 273−285.
(38) Hamm, P.; Hochstrasser, R. M. Structure and Dynamics of Proteins and Peptides: Femtosecond Two-Dimenaional Infrared Spectroscopy. In *Ultrafast Infrared And Raman Spectroscopy*; Fayer, M. D., Ed.; Marcel Dekker: New York, 2001; pp 273−347.
(39) Shim, S.-H.; Strasfeld, D. B.; Fulmer, E. C.; Zanni, M. T. Femtosecond Pulse Shaping Directly in the Mid-IR Using Acousto-Optic Modulation. *Opt. Lett.* **2006**, *31*, 838−840.
(40) Shim, S.-H.; Strasfeld, D. B.; Zanni, M. T. Generation and Characterization of Phase and Amplitude Shaped Femtosecond Mid-IR Pulses. *Opt. Express* **2006**, *14*, 13120−13130.
(41) Nite, J. M.; Cyran, J. D.; Krummel, A. T. Active Bragg Angle Compensation for Shaping Ultrafast Mid-Infrared Pulses. *Opt. Express* **2012**, *20*, 23912.
(42) Shim, S.-H.; Zanni, M. T. How to Turn Your Pump−probe Instrument into a Multidimensional Spectrometer: 2D IR and Vis Spectroscopies via Pulse Shaping. *Phys. Chem. Chem. Phys.* **2009**, *11*, 748−761.
(43) Frisch, M. J.; Trucks, G. W.; Schlegel, H. B.; Scuseria, G. E.; Robb, M. A.; Cheeseman, J. R.; Scalmani, G.; Barone, V.; Mennucci, B.; Petersson, G. A.; et al. *Gaussian 09*, revision D.01; Gaussian, Inc.: Wallingford, CT, 2009.
(44) Andersson, M. P.; Uvdal, P. New Scale Factors for Harmonic Vibrational Frequencies Using the B3LYP Density Functional Method with the Triple-Z Basis Set 6-311+G(d,p). *J. Phys. Chem. A* **2005**, *109*, 2937−2941.
(45) Josien, M.-L.; Fuson, N.; Lebas, J.-M.; Gregory, T. M. An Infrared Spectroscopic Study of the Carbonyl Stretching Frequency in a Group of Ortho and Para Quinones. *J. Chem. Phys.* **2004**, *21*, 331−340.
(46) Anno, T. Molecular Vibrations of Quinones. V. Normal Coordinate Analysis of P-Benzoquinone and Its Isotopic Derivatives. *J. Chem. Phys.* **1965**, *42*, 932.
(47) Dunn, T. M.; Francis, A. H. The Ground State Fundamentals of P-Benzoquinone and P-Benzoquinone-d4. *J. Mol. Spectrosc.* **1974**, *50*, 1−13.
(48) Singh, S. N.; Singh, R. S. Vibrational Spectra of Condensed Ring quinones—I 1,4-Naphthoquinone and 9,10-Anthraquinone. *Spectrochim. Acta, Part A* **1968**, *24*, 1591−1597.
(49) Wilson, E. B.; Decius, J. C.; Cross, P. C. *Molecular Vibrations: The Theory of Infrared and Raman Vibration Spectra*; Dover: Mineola, NY, 1980.

DOI: 10.1021/jp506900n
J. Phys. Chem. B XXXX, XXX, XXX−XXX